
PERGAMON

Journal of Quantitative Spectroscopy & Radiative Transfer 73 (2002) 409–421

Journal of Quantitative Spectroscopy & Radiative Transfer

www.elsevier.com/locate/jqsrt

Effects of gas and soot radiation on soot formation in a coflow laminar ethylene diffusion flame

Fengshan Liu *, Hongsheng Guo, Gregory J. Smallwood, Ömer L. Gülder[1]

Combustion Research Group, Institute for Chemical Process and Environmental Technology, National Research Council Canada, Building M-9, Montreal Road, Ottawa, Canada, K1A 0R6

Received 3 August 2001

Abstract

A computational study of soot formation in an undilute axisymmetric laminar ethylene-air coflow jet diffusion flame at atmospheric pressure was conducted using a detailed gas-phase reaction mechanism and complex thermal and transport properties. A simple two-equation soot model was employed to predict soot formation, growth, and oxidation with interactions between the soot chemistry and the gas-phase chemistry taken into account. Both the optically thin model and the discrete-ordinates method coupled with a statistical narrow-band correlated-K based wide band model for radiative properties of CO, CO_2, H_2O, and soot were employed in the calculation of radiation heat transfer to evaluate the adequacy of using the optically thin model. Several calculations were performed with and without radiative transfer of radiating gases and/or soot to investigate their respective effects on the computed soot field and flame structure. Radiative heat transfer by both radiating gases and soot were found to be important in this relatively heavily sooting flame studied. Results of the optically thin radiation model are in good agreement with those obtained using the wide band model except for the flame temperature near the flame tip.

1. Introduction

Soot formed in the fuel rich regions of hydrocarbon diffusion flames plays an important role in flame radiation and fire spread through the mechanism of radiation heat transfer. It is therefore, of great importance to develop modeling capabilities to accurately predict soot formation in flames in order to effectively control soot in practical applications. Despite the significant progress made

* Corresponding author. Fax: +1-613-957-7869.

E-mail address: fengshan.liu@nrc.ca (F. Liu).

[1] Now at: University of Toronto, Institute for Aerospace Studies, 4925 Dufferin Street, Toronto, Ontario, Canada, M3W 5T6.

0022-4073/02/$ - see front matter.
PII: S0022-4073(01)00205-9

towards the understanding of the mechanisms of soot inception, growth and oxidation in the last three to four decades, these processes have not been fully understood. Consequently, no universal soot model exists that is equally applicable for different fuels and for different operating conditions. The detailed soot models developed by Frenklach and co-workers [1–3] consider some 600 elementary reactions and 200 species and such models are currently not feasible to be implemented into a multidimensional flame code to predict soot formation. Various semi-empirical soot models have been developed, improved and used extensively in laminar flame [4–15] and turbulent flame [16–19] calculations with some success.

Detailed calculations of generic multidimensional laminar diffusion flames are beyond currently available capabilities due to limited computer resources. On the other hand, numerical calculations in one-dimensional counterflow flames, though simple and relatively easy to compute, are not adequate or even impossible to validate some important aspects of soot models such as the visible flame height, coupling of radiation and soot concentration, and the effect of a multidimensional flow field. The strong coupling between soot and radiation should be studied in multidimensional flames since radiation is inherently a multidimensional phenomenon. The two-dimensional axisymmetric coflow laminar jet diffusion flame is an ideal configuration to study these processes since it is simple enough to allow numerical calculations using detailed gas-phase chemistry and complex transport and thermal properties. Therefore, considerable research efforts have been undertaken to model soot formation in axisymmetric coflow jet diffusion laminar flames using simplified soot formation models.

Accurate calculations of soot formation in multidimensional flames are very challenging since each of the physical and chemical process involved needs to be correctly modeled. The phenomena associated with soot formation and oxidation include fluid dynamics, complex transport and thermal properties of species, finite rate chemistry of gaseous reactions, finite rate chemistry of soot processes, and non-grey radiation heat transfer by soot and gaseous species. While the importance of the coupling of radiation and soot kinetics in sooting flames has been recognized and demonstrated in the studies mentioned above, these studies either employed detailed gas-phase chemistry but the simple optically thin model for radiation [10,13–15] or very crude gas-phase chemistry and a more sophisticated treatment for radiation [8,12]. Modeling of soot formation in a coflow laminar diffusion flame using both a detailed gas-phase chemistry and a non-grey radiation model has not been reported, perhaps due to the complexity of the problem. Although it is true that gas radiation is dominant over soot radiation in lightly sooting flames [12] and the opposite may be true for heavily sooting flame, the relative importance of gas radiation and soot radiation in a moderately sooting flame has not been investigated. In addition, the use of the optically thin model in modeling such a flame has not been quantitatively evaluated.

In the present study, numerical calculations of soot formation in an axisymmetric coflow laminar diffusion ethylene-air flame at atmospheric pressure were conducted using a modified version of the two-equation soot model of Leung et al. [5] to predict soot formation, growth and oxidation. This moderately sooting diffusion flame was chosen for the reason that radiation heat transfer by both radiating gases and soot could be important. Computationally, we employed the primitive variable method in which the fully elliptic governing equations for conservation of mass, momentum, energy, gaseous species and soot mass fraction and number density were solved with detailed gas-phase chemistry and complex thermal and transport properties. The effects of soot inception, growth and oxidation on gas-phase chemistry were accounted for. Radiation heat transfer was calculated using both the optically thin model and the discrete-ordinates method coupled with a statistical narrow-band

correlated-K (SNBCK)-based wide band model for radiative properties of CO, CO_2, H_2O and soot. The objectives of this study are (1) to provide a quantitative evaluation of the optically thin model, and (2) to quantify the relative importance of gas radiation and soot radiation.

2. Model formulation and numerical method

2.1. Governing equations

The governing equations of mass, momentum, energy and species in axisymmetric cylindrical coordinates (r,z) given in Ref. [20] were solved in the present study. The gravitational term is included in the momentum equation. Correction velocities are used to ensure that the mass fractions sum to unity. The thermophoretic velocities of soot are included in the calculation of the correction velocities.

2.2. Soot model

A modified version of the semi-empirical two-equation formulation of soot kinetics [5] was used to model soot nucleation, growth and oxidation. The transport equations for the soot mass fraction and number density are given as

$$\rho v\frac{\partial Y_s}{\partial r}+\rho u\frac{\partial Y_s}{\partial z}=-\frac{1}{r}\frac{\partial}{\partial r}(r\rho V_{T,r}Y_s)-\frac{\partial}{\partial z}(\rho V_{T,z}Y_s)+S_m, \tag{1}$$

$$\rho v\frac{\partial N}{\partial r}+\rho u\frac{\partial N}{\partial z}=-\frac{1}{r}\frac{\partial}{\partial r}(r\rho V_{T,r}N)-\frac{\partial}{\partial z}(\rho V_{T,z}N)+S_N, \tag{2}$$

where Y_s is the soot mass fraction and N is the soot number density defined as the particle number per unit mass of mixture. Quantities $V_{T,r}$ and $V_{T,z}$ are the thermophoretic velocities of soot in the r and z directions, respectively, and are calculated as

$$V_{T,x_i}=-0.65\frac{\mu}{\rho T}\frac{\partial T}{\partial x_i}\quad x_i=r,z. \tag{3}$$

The source term S_m in Eq. (1) accounts for the effects of soot nucleation, surface growth and oxidation. The simplified soot nucleation and growth mechanisms proposed by Leung et al. [5] were followed which assume that acetylene is the only soot nucleation and growth species. The rates of nucleation and growth are given as

$$R_1=k_1(T)[C_2H_2],\quad (\mathrm{kmol/m^3/s}), \tag{4}$$

$$R_2=k_2(T)f(A_s)[C_2H_2],\quad (\mathrm{kmol/m^3/s}), \tag{5}$$

where $f(A_s)$ denotes the functional dependence of soot surface growth on soot surface area per unit volume and $[C_2H_2]$ is the mole concentration of acetylene. Following Leung et al. [5], we assume that the functional dependence is a square root relation, i.e. $f(A_s)=A_s^{0.5}$. The soot surface

area per unit volume is calculated as $A_s = \pi(6/\pi)^{2/3}\rho_{C(S)}^{-2/3}Y_s^{2/3}\rho N^{1/3}$ with the density of soot $\rho_{C(S)}$ taken to be 1900 kg/m^3. The nucleation and growth rates used in the present calculations are: $k_1 = 1000\exp(-16103/T)$ (1/s) and $k_2 = 1750\exp(-10064/T)$ (m$^{0.5}$/s). These rate constants are different from those used by Leung et al. [5] and Fairweather et al. [16] for the reason given below.

Neoh et al. [21] have investigated soot oxidation process in flames and found that the oxidation of soot by both O_2 and OH is important and the relative importance of O_2 and OH depend on the local equivalence ratio. The O radical also contributes to soot oxidation in some regions [22]. Therefore soot oxidation by all these three oxidative agents was taken into account in the present study. Soot oxidation was assumed to proceed through the following reactions:

$$0.5\,O_2 + C(S) \rightarrow CO,$$

$$OH + C(S) \rightarrow CO + H,$$

$$O + C(S) \rightarrow CO.$$

The reaction rates per unit surface area of these three reactions (kg m^{-2}s^{-1}) are given as

$$R_3 = 120\left\{\frac{k_A X_{O_2}\chi}{1 + k_Z X_{O_2}} + k_B X_{O_2}(1-\chi)\right\}, \quad \chi = \left\{1 + \frac{k_T}{k_B X_{O_2}}\right\}^{-1}, \tag{6}$$

$$R_4 = \varphi_{OH} k_4(T) T^{-1/2} X_{OH}, \tag{7}$$

$$R_5 = \varphi_O k_5(T) T^{-1/2} X_O, \tag{8}$$

where X_{OH} and X_O denote the mole fractions of OH and O, and φ_{OH} and φ_O are the collision efficiencies for OH and O attacking on soot particles. The rate of soot oxidation by O_2 was based on the Nagle–Strickland–Constable model [23] with rate constants for R_3 and R_4 taken from Ref. [9]. The constant collision efficiency of 0.2 was assumed for both OH and O. The rate constants for R_5 were taken from Ref. [22].

The source term S_N in Eq. (2) represents the production and destruction of the number density of soot particles due to nucleation and agglomeration and is written as [5]

$$S_N = \frac{2}{C_{min}} N_A R_1 - 2C_a\left(\frac{6M_{C(S)}}{\pi\rho_{C(S)}}\right)^{1/6}\left(\frac{6\kappa T}{\rho_{C(S)}}\right)^{1/2}[C(s)]^{1/6}[\rho N]^{11/6} \tag{9}$$

where N_A is Avogadro's number (6.022×10^{26} particles/kmol), κ is the Boltzman constant (1.38×10^{-23} J/K), C_{min} is the number of carbon atoms in the incipient carbon particle (700, which gives a soot inception particle diameter of about 2.4 nm), and C_a is the agglomeration rate constant. The typical values of C_a used in the literature are 3 [11,16] and 9 [5,19]. Almost all the present soot models assume that the soot number density decreases as a result of particle agglomeration into spherical aggregates. The only exception is perhaps the study of Ezekoye and Zhang [11] who investigated the effect of particle agglomeration by setting C_a to zero, i.e. to neglect particle agglomeration. It has been established experimentally that soot aggregates consist of more or less identical primary soot particles and the primary soot particle number density remains almost constant in the growth region [24]. In other words, primary soot particle coalescence (collisional growth to form spherical clusters) is not important and can be neglected. These experimental findings suggest

that it is more realistic to neglect the destruction term of the soot number density by setting C_a to zero.

The density of the mixture (including soot) was calculated using the following state equation

$$\rho = \frac{p_a}{R_u T \sum_{k=1}^{KK} Y_k/W_k}, \tag{10}$$

where p_a is the ambient pressure (1 atm in this study), R_u the universal gas constant, and KK the number of gas-phase species considered.

2.3. Radiation model

In the present study, the radiation source term in the energy equation was obtained using the discrete-ordinates method in axisymmetric cylindrical geometry described by Truelove [25]. The T_3 quadrature [26,27] was used for the angular discretisation. Spatial discretisation of the transfer equation was achieved using the finite volume method along with the central difference scheme.

SNBCK based wide band model developed by Liu et al. [28,29] was employed to obtain the absorption coefficients of the combustion products containing CO, CO_2 and H_2O at each wide band. The spectral absorption coefficient of soot was assumed to be $5.5 f_v/\lambda$ with f_v being the soot volume fraction and λ the wavelength. The wide bands considered in the calculations were formed by lumping 10 successive uniform narrowbands of 25 cm^{-1}, giving a bandwidth of 250 cm^{-1} for each wide band. The blackbody intensity at each wide band was evaluated at the band centre. The SNB parameters for CO, CO_2 and H_2O were those compiled by Soufiani and Taine [30] based on line-by-line calculations. At overlapping bands, the approximate treatment based on the optically thin limit developed by Liu et al. [31] was employed. To further speed up the calculations without losing accuracy, the 4-point Gaussian–Legendre quadrature was used to invert the cumulative distribution function to obtain the absorption coefficients based on the findings of Liu et al. [32]. The radiation source term was calculated by summing up contributions of all the 36 wide bands (from 150 to 9150 cm^{-1}) considered in the calculations.

To evaluate the results of the optically thin model using those of the wide band model discussed above, numerical calculations were also conducted using the optically thin radiation model. Under the optically thin approximation, the radiation source term is calculated as

$$q_r = -C f_v T^5 - k_p 4\sigma T^4, \tag{11}$$

where C is a constant (3.337×10^{-10} which gives a power density in watts/cm^3) calculated based on the spectral absorption coefficient of soot, σ the Stefan–Boltzmann constant and k_p the Planck mean absorption coefficient of the gas mixture including contributions from CO, CO_2 and H_2O. The Planck mean absorption coefficients of these three species used in this work were calculated based on the SNB model given in Ref. [33].

2.4. Numerical method

The transport equations for mass, momentum, energy, gas-phase species, soot mass fraction, soot number density, and radiation intensity are closed with the equation of state and appropriate boundary conditions on each side of the computational domain. Diffusion terms in the conservation equations

are discretized by the central difference scheme and convective terms are discretized by the upwind difference scheme. The SIMPLE numerical algorithm [34] was used to treat the pressure and velocity coupling. Governing equations of momentum, energy, soot mass fraction and number density were solved using the tridiagonal-matrix algorithm. Governing equations of the gas-species were solved in a fully coupled fashion at every grid using a direct solver to speed up the convergence process [35].

The gas-phase reaction mechanism used was basically GRI-Mech 3.0 [36]. The only modification is the removal of all the reactions and species related to NO_X formation. The revised reaction scheme consists of 36 species and 219 reactions. All the thermal and transport properties are obtained by using the database of GRI-Mech 3.0 and the CHEMKIN codes.

3. Results and discussions

The laminar axisymmetric coflow C_2H_4-air diffusion flame at atmospheric pressure calculated in this study had been previously investigated experimentally in our laboratory [37,38]. The flame was generated with a burner in which pure ethylene flows through an uncooled 10.9 mm inner diameter vertical steel tube and the air flows from the annular region between the fuel tube and a 100 mm inner diameter concentric tube. The wall thickness of the fuel tube is 0.95 mm. The volume flow rates of the fuel and the air are 194 ml/min and 284 l/min, respectively. Both fuel and air are delivered at room temperature (294 K).

The experimental results of Gülder et al. [38] show that the outer surface temperature of the fuel pipe was about 100 K higher than the room temperature due to flame heating, which imply that the fuel and air are heated to a temperature higher than 294 K due to heat conduction from the fuel pipe. Such a preheating effect was not considered. The computational grids and boundary conditions used in the calculations are shown in Fig. 1. Non-uniform grids were used in both r and z directions to provide greater resolution in the large gradient regions without an excessive increase in the computing time. Very fine grids were placed between 0 and 1.2 cm in r direction. The computational domain consists of 102×60 cells. A parabolic laminar pipe flow velocity profile was assigned to the inlet velocity of the fuel stream. For the air stream, a boundary layer velocity profile was assumed inside the boundary layer (formed along the outer surface of the fuel pipe) and the uniform velocity was prescribed outside it. Unless otherwise stated, the SNBCK based wide band model was used to obtain the results presented below. The convergence criterion used in the calculations is that relative change of the peak soot volume fraction is less than 1×10^{-5}.

Fig. 2 shows the measured [38] (using the CARS technique) and the predicted fields of temperature with various treatments of radiation heat transfer. The corresponding distributions of soot volume fraction are compared in Fig. 3 with the maximum soot volume fraction indicated in each case. The experimental soot volume fractions were obtained using the laser extinction/Abel inversion technique. The predicted temperature field with both gas and soot radiation accounted for, Fig. 2(b), is in qualitative agreement with the measured one. However, the predicted peak flame temperature (2015 K) and temperatures in the centerline region are more than 100 K lower than the measured values. In addition, the calculated maximum temperature annulus is thinner than the experimental one. The causes of these discrepancies may be attributed to (i) the effect of fuel preheating as mentioned above and (ii) use of the simplified soot model. The peak temperature predicted using the optically

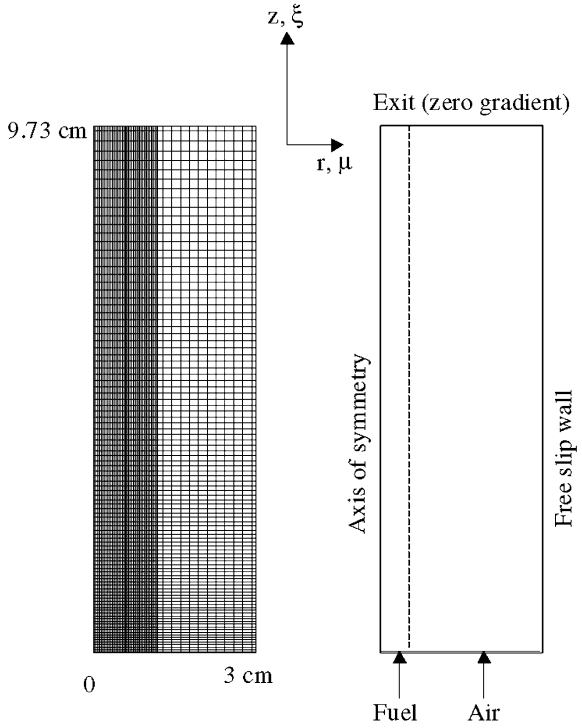

Fig. 1. Computational grid and schematic of the solution domain and boundary conditions.

thin model, Fig. 2(c), is only about 5 K lower than that of the band model. The centerline region temperatures are also underpredicted mainly due to neglect of radiation absorption by CO_2 and to a lesser degree by CO, especially in CO burnout regions right above the flame tip (around and above $z = 6$ cm) where the concentration of CO_2 is very high. The optically thin model underpredicts the temperature in these regions by more than 50 K compared to the band model results.

When radiation by gases is neglected, Fig. 2(d), the predicted temperature levels are in reasonably good agreement with those in Fig. 2(b). However the peak flame temperature is now about 30 K higher and the temperatures in the upper central regions above $z = 3$ cm are also significantly higher by about 80 K, indicating that radiation by gases is also important and should be accounted for in the flame investigated. The hot spot at the centerline region at about $z = 6.4$ cm is a direct consequence of CO to CO_2 conversion and the neglect of heat loss by CO_2 radiation. The increased peak flame temperature at the lower annular region is attributed to the neglect of radiation heat loss by H_2O whose concentration distributions correlate very well with temperature distributions.

Comparison of results shown in Figs. 2(d)–(f) suggests that soot radiation is more important than gas radiation in this flame since it has a greater impact on the predicted temperature distributions. Neglect of soot radiation results in significantly higher temperatures at upper portion of the flame above $z = 2$ cm. If radiation by both the gases and soot is neglected, Fig. 2(f), the peak flame temperature is about 123 K higher and temperatures in the upper centerline region are about 400 K higher than those in Fig. 2(b).

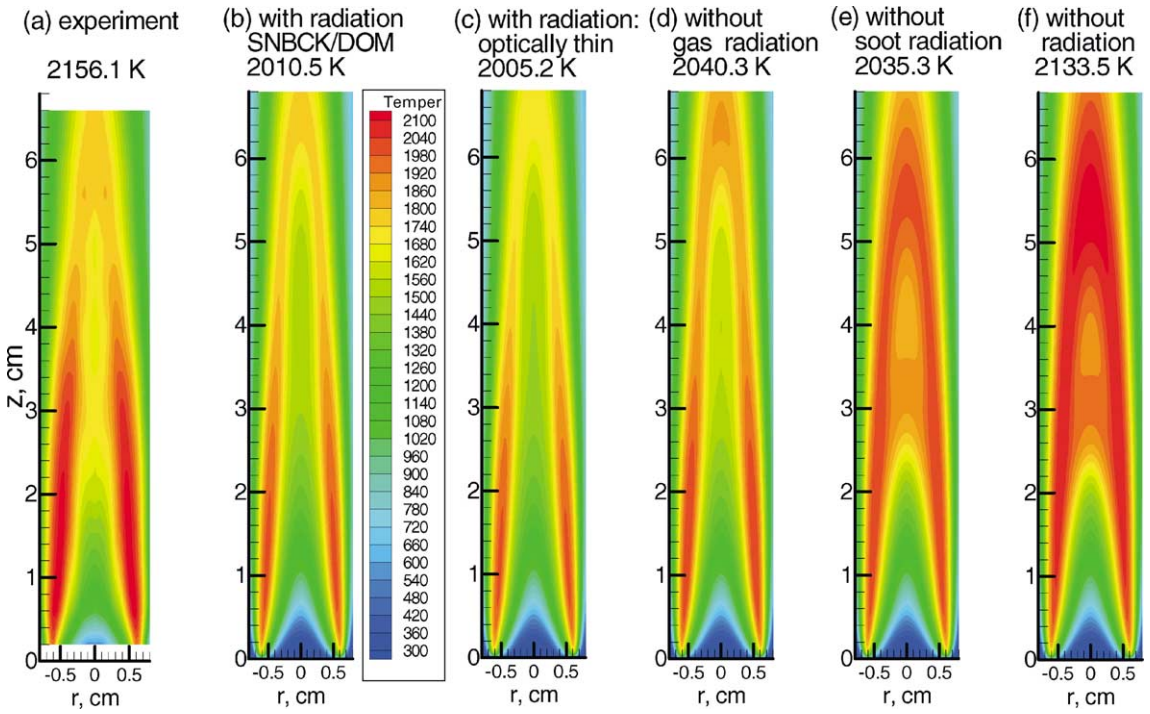

Fig. 2. Comparison of measured and predicted temperature distributions with the peak values indicated.

The predicted distributions of soot volume fraction, Fig. 3(b), are in qualitative agreement with the measurement, Fig. 3(a). The peak values are in very good agreement. The major discrepancies between the prediction and the measurement are: (i) the predicted high-concentration soot annulus is thicker than the measured one, (ii) the predicted soot concentrations in the centerline region are much lower than the experiment and do not converge as in the experiment, and (iii) the predicted visible flame height is lower, which is believed to be the consequence of (ii). Use of the optically thin model, Fig. 3(c), leads to a lower peak soot volume fraction and a slightly higher visible flame height. Neglect of gas radiation only, Fig. 3(d), results in a much higher peak soot volume fraction and a slightly lower flame height. While neglect of soot radiation only, Fig. 3(e), does not significantly affect the peak soot volume fraction. However, the visible flame height is greatly reduced. If radiation by both gas and soot is neglected, Fig. 3(f), the visible flame height is further reduced and the peak soot volume fraction is higher compared to those in Figs. 3(b) and (e).

Results shown in Fig. 3 indicate that neglect of gas radiation significantly increases the peak soot volume fraction but only slightly reduces the visible flame height. In contrast, neglect of soot radiation significantly reduces the flame height but only slightly lowers the peak soot volume fraction. Since soot distributions are the result of two competing processes: soot formation (nucleation and growth) and soot oxidation, it is important to analyze how gas and soot radiation affect these processes in order to understand the results shown in Fig. 3. The predicted rates of soot nucleation, growth, and oxidation by OH are shown in Figs. 4–6. The OH oxidation mechanism was found to be the dominant one in the present study. The rate of soot oxidation by OH is an order of magnitude

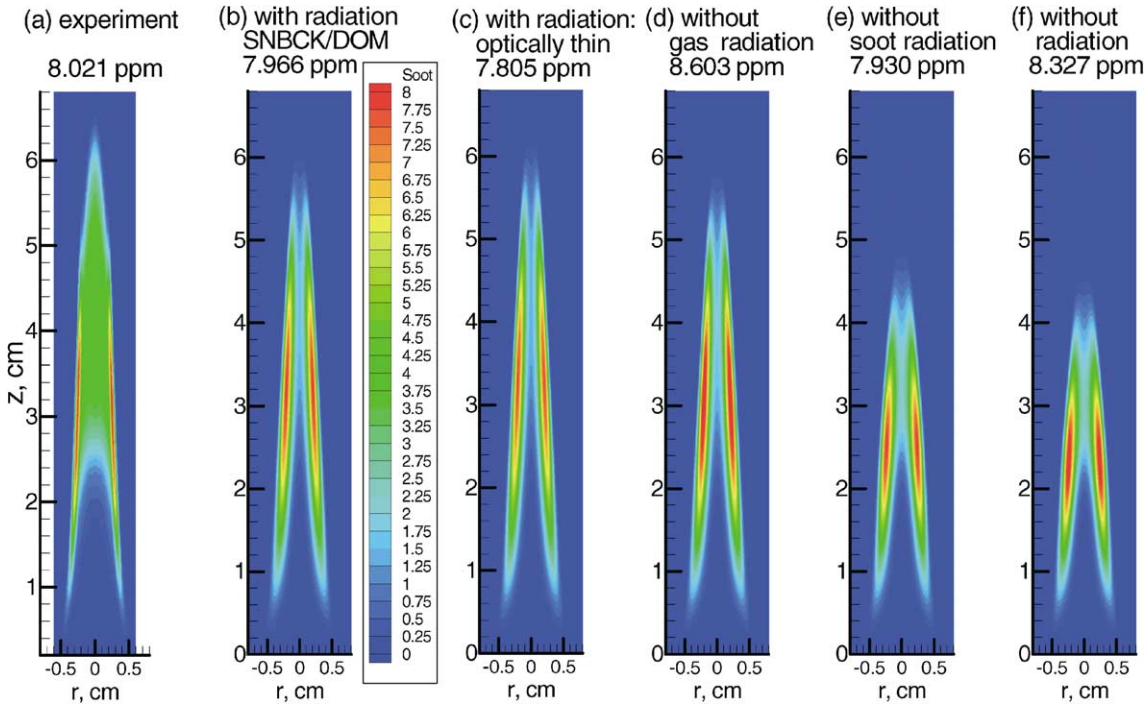

Fig. 3. Comparison of measured and predicted soot volume fraction distributions with the peak values indicated.

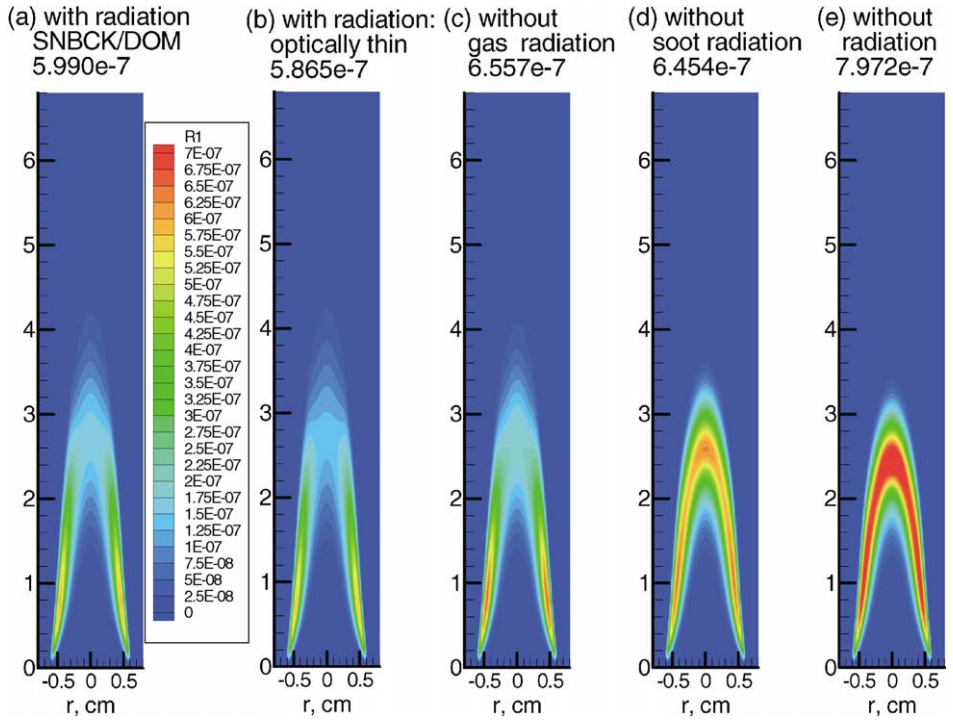

Fig. 4. Comparison of predicted soot nucleation rates in g cm^{-3} s^{-1} with the peak values indicated.

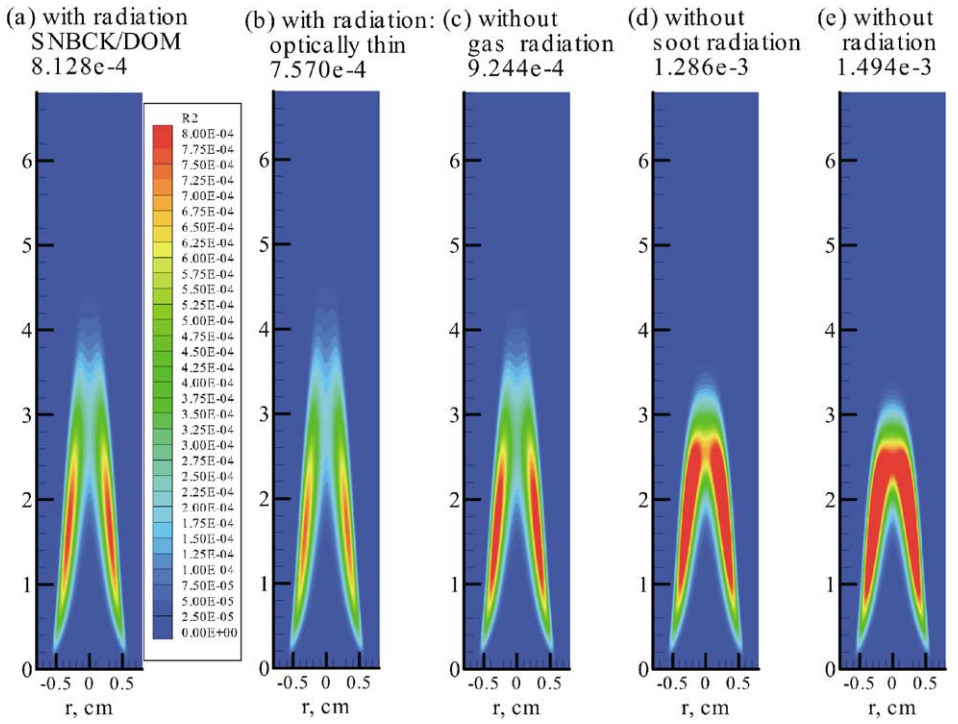

Fig. 5. Comparison of predicted soot growth rates in g cm^{-3} s^{-1} with the peak values indicated.

higher than that by O atom and about two orders of magnitude higher than that by O_2. As mentioned earlier, the high-concentration regions of the three radiating gases are in different parts of the flame: H_2O is in the lower annular region of the high temperatures, CO_2 is in the upper part of the flame tip (centerline region), and CO is just below CO_2 and is formed by soot burnout. Therefore, gas radiation affects the flame temperatures in these regions. It is seen from Figs. 4 and 5 that soot nucleation and growth primarily occur in the inner region of the high-temperature annulus below about $z = 3$ cm. Therefore, gas radiation affects soot nucleation and growth through radiation heat loss by H_2O in soot nucleation and growth regions. Neglect of gas radiation increases rates of soot nucleation and growth, Figs. 4(c) and 5(c), especially the growth rate. However, the rate of soot oxidation by OH in the upper part of the flame is only slightly increased, compare Figs. 6(a) and (c). This is why neglect of gas radiation results in a much higher peak soot volume fraction and a slightly shorter visible flame height as shown in Fig. 3(d). On the other hand, soot radiation primarily affects the flame temperatures in the upper part of the flame roughly above $z = 2$ cm, Fig. 2(e). Therefore neglect of soot radiation enhances the rates of every process of soot, i.e. nucleation, growth, and oxidation, at relatively upper part of the flame above $z = 2$ cm. When soot radiation is neglected, not only the peak soot oxidation rate by OH increases, Fig. 6(d), but also the region of high soot oxidation rate appears at a distance much closer to the burner exit, leading to a reduced residence time for soot particles to grow. The combined effects of soot radiation on rates of soot nucleation, growth, and oxidation explain why neglect of soot radiation yields a much short visible

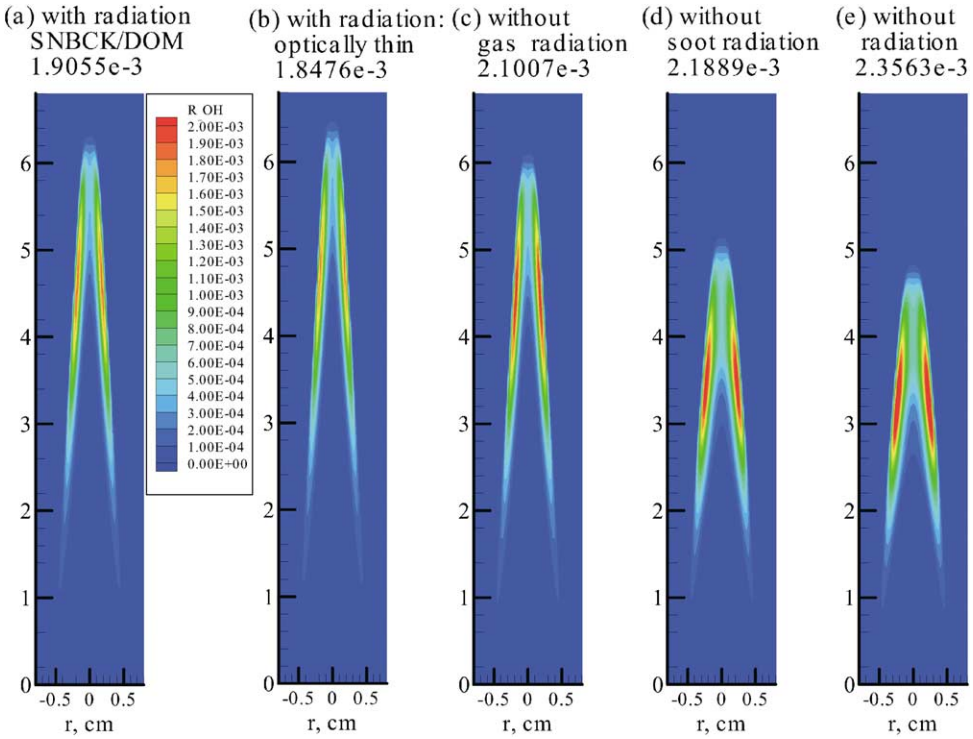

Fig. 6. Comparison of predicted soot oxidation rates by OH in g cm^{-3} s^{-1} with the peak values indicated.

flame height, a lower high-concentration soot annulus and an almost unaffected peak soot volume fraction.

4. Conclusions

Numerical simulation of a coflow laminar diffusion C_2H_4-air flame at atmospheric pressure by a detailed gas-phase reaction mechanism, complex transport and thermal properties, and a simplified two-equation soot model was conducted. Numerical results show that the simulation captured the main features of the flame temperature and soot distributions. Soot nucleation, growth, and oxidation are all affected by gas and soot radiation. The effect of gas radiation on soot nucleation and growth is greater relative to its effect on soot oxidation. Neglect of gas radiation yields about an 8% higher peak soot volume fraction and a slightly shorter visible flame height. Soot radiation is clearly more important than gas radiation in the flame investigated. Soot radiation affects soot oxidation by OH more than its effect on soot nucleation and growth through enhanced OH concentrations. Neglect of soot radiation leads to a much shorter visible flame height due to rapid soot burnout and an almost unaffected peak soot volume fraction as a results of two competing mechanisms: enhanced rates of soot nucleation and growth and reduced residence time for growth as a result of increased soot oxidation by OH. Use of the optically thin radiation model predicts a slightly lower (about 2%) peak soot volume fraction and a slightly higher visible flame height. The temperatures in the upper

centerline region above the flame tip predicted by this model are more than 50 K lower, which may have a significant impact on the calculation of NO_x emission from this flame. Overall results of the optically thin model are in good agreement with those of the band model in the calculation of the flame studied.

References

[1] Frenklach M, Clary DW, Gardiner Jr. WC, Stein SE. Detailed kinetics modeling of soot formation in shock-tube pyrolysis of acetylene. 20th International Symposium on Combustion. Pittsburgh: The Combustion Institute, 1984. p. 887–901.
[2] Frenklach M, Wang H. Detailed modeling of soot particle nucleation and growth. Proceedings of the 23rd International Symposium on Combustion. Pittsburgh: The Combustion Institute, 1990, p. 1559–66.
[3] Frenklach M, Wang H. Detailed mechanism and modeling of soot particle formation. In: Bockhorn H, editor. Soot formation in combustion: mechanisms and models. Springer Series in Chemical Physics, vol. 59. Berlin: Springer, 1994. p. 162–90.
[4] Kennedy IM, Kollmann W, Chen JY. A model for soot formation in a laminar diffusion flame. Combust Flame 1990;81:73–85.
[5] Leung KM, Lindstedt RP, Jones WP. A simplified reaction mechanism for soot formation in nonpremixed flames. Combust Flame 1991;87:289–305.
[6] Stewart CD, Syed KJ, Moss JB. Modelling soot formation in non-premixed kerosine-air flames. Combust Sci Technol 1991;75:211–26.
[7] Kaplan CR, Baek SW, Oran ES, Ellzey JL. Dynamics of a strongly radiating unsteady ethylene jet diffusion jet. Combust Flame 1994;96:1–21.
[8] Sivathanu YR, Gore JP. Coupled radiation and soot kinetics calculations in laminar acetylene/air diffusion flames. Combust Flame 1994;97:161–72.
[9] Moss JB, Stewart CD, Young KJ. Modeling soot formation and burnout in a high temperature laminar diffusion flame burning under oxygen-enriched conditions. Combust Flame 1995;101:491–500.
[10] Kennedy IM, Yam C, Rapp DC, Santoro RJ. Modeling and measurements of soot and species in a laminar diffusion flame. Combust Flame 1996;107:368–82.
[11] Ezekoye OA, Zhang Z. Soot oxidation and agglomeration modeling in a microgravity diffusion flame. Combust Flame 1997;110:127–39.
[12] Sivathanu YR, Gore JP. Effects of gas-band radiation on soot kinetics in laminar methane/air diffusion flames. Combust Flame 1997;110:256–63.
[13] Kaplan CR, Patnaik G, Kailasanath K. Universal relationships in sooting methane-air diffusion flames. Combust Sci Technol 1998;131:39–65.
[14] McEnally CS, Schaffer AM, Long MB, Pfefferle LD, Smooke MD, Colket MB, Hall RJ. Computational and experimental study of soot formation in a coflow, laminar ethylene diffusion flame. Proceedings of the 27th International Symposium on Combustion. Pittsburgh: The Combustion Institute, 1998. p. 1497–505.
[15] Smooke MD, McEnally CS, Pfefferle LD, Hall RJ, Colket MB. Computational and experimental study of soot formation in a coflow, laminar diffusion flame. Combust Flame 1999;117:117–39.
[16] Fairweather M, Jones WP, Lindstedt RP. Predictions of radiative transfer from a turbulent reacting jet in a cross-wind. Combust Flame 1992;89:45–63.
[17] Fairweather M, Jones WP, Ledin HS, Lindstedt RP. Predictions of soot formation in turbulent, non-premixed propane flames. Proceedings of the 24th International Symposium on Combustion. Pittsburgh: The Combustion Institute, 1992. p. 1067–74.
[18] Brookes SJ, Moss JB. Predictions of soot and thermal radiation properties in confined turbulent jet diffusion flames. Combust Flame 1999;116:486–503.
[19] Kronenburg A, Bilger RW, Kent JH. Modeling soot formation in turbulent methane-air jet diffusion flames. Combust Flame 2000;121:24–40.
[20] Kuo KK. Principles of Combustion. New York: Wiley, 1986. p. 172–205.

[21] Neoh KG, Howard JB, Sarofim AF. Soot oxidation in flames. In: Siegla DC, Smith GW, editors. Particulate carbon: formation during combustion. New York: Plenum, 1981. p. 261–77.
[22] Bradley D, Dixon-Lewis G, Habik SE, Mushi EMJ. The oxidation of graphite powder in flame reaction zones. Proceedings of the 20th International Symposium on Combustion. Pittsburgh: The Combustion Institute, 1984. p. 931–40.
[23] Nagle J, Strickland-Constable RF. Oxidation of carbon between 1000–2000°C. Proceedings of the Fifth Conference on Carbon. London: Pergamon Press, 1962. p. 154–64.
[24] Megaridis CM, Dobbins RA. Comparison of soot growth and oxidation in smoking and non-smoking ethylene diffusion flames. Combust Sci Technol 1989;66:1–16.
[25] Truelove JS. Evaluation of a multi-flux model for radiative heat transfer in cylindrical furnaces. AERE-R-9100, AERE, Harwell, UK, 1978.
[26] Thurgood CP. A critical evaluation of the discrete ordinates method using HEART and T_N quadrature, Ph.D thesis, Queen's University at Kingston, Ontario, Canada, 1992.
[27] Thurgood CP, Becker HA, Pollard A. The T_N quadrature set for the discrete-ordinates method. J Heat Transfer 1995;117:1068–70.
[28] Liu F, Smallwood GJ, Gülder ÖL. Radiation heat transfer calculations using the SNBCK method. AIAA paper 99–3679.
[29] Liu F, Smallwood GJ, Gülder ÖL. Band lumping strategy for radiation heat transfer calculations using a narrowband model. J Thermophys Heat Transfer 2000;14:278–81.
[30] Soufiani A, Taine J. High temperature gas radiative property parameters of statistical narrow-band model for H_2O, CO_2 and CO, and correlated-K model for H_2O and CO_2. Int J Heat Mass Transfer 1997;40:987–91.
[31] Liu F, Smallwood GJ, Gülder ÖL. Application of the statistical narrow-band correlated-K method to non-grey gas radiation in CO_2–H_2O mixtures: approximate treatments of overlapping bands. JQSRT 2001;68:401–17.
[32] Liu F, Smallwood GJ, Gülder ÖL. Application of the statistical narrow-band correlated-K method to low-resolution spectral intensity and radiative heat transfer calculations—effects of the quadrature scheme. Int J Heat and Mass Transfer 2000;43:3119–35.
[33] Ju Y, Guo H, Liu F, Maruta K. Effects of the Lewis number and radiative heat loss on the bifurcation and extinction of CH_4/O_2–N_2–He flames. J Fluid Mech 1999;379:165–90.
[34] Patankar SV. Numerical heat transfer and fluid flow. New York: Hemisphere, 1980.
[35] Liu Z, Liao C, Liu C, McCormick S. Multigrid method for multi-step finite rate combustion. AIAA 95-0205, 1995.
[36] Smith GP, Golden DM, Frenklach M, Moriarty NW, Eiteneer B, Goldenberg M, Bowman CT, Hanson RK, Song S, Gardiner WC Jr., Lissianski VV, Qin Z. URL: http://www.me.berkeley.edu/gri_mech/.
[37] Snelling DR, Thomson KA, Smallwood GJ, Gülder ÖL. Two-dimensional imaging of soot volume fraction in laminar diffusion flames. Appl Opt 1999;38:2478–85.
[38] Gülder ÖL, Thomson KA, Snelling DR. Influence of the fuel nozzle material on soot formation and temperature field in coflow laminar diffusion flames. Paper presented at The Combustion Institute Canadian Section 2000 Spring Technical Meeting, University of Ottawa, Ottawa, ONT, 2000.